PNAS RESEARCH ARTICLE | MICROBIOLOGY OPEN ACCESS

Genome-wide CRISPRi screen identifies enhanced autolithotrophic phenotypes in acetogenic bacterium *Eubacterium limosum*

Jongoh Shin[a,1], Jiyun Bae[a,1], Hyeonsik Lee[a], Seulgi Kang[a], Sangrak Jin[a], Yoseb Song[a], Suhyung Cho[a,b], and Byung-Kwan Cho[a,b,2]

Edited by Jens Nielsen, BioInnovation Institute, Copenhagen, Denmark; received September 22, 2022; accepted January 6, 2023

Acetogenic bacteria are a unique biocatalyst that highly promises to develop the sustainable bioconversion of carbon oxides (e.g., CO and CO_2) into multicarbon biochemicals. Genotype–phenotype relationships are important for engineering their metabolic capability to enhance their biocatalytic performance; however, systemic investigation on the fitness contribution of individual gene has been limited. Here, we report genome-scale CRISPR interference screening using 41,939 guide RNAs designed from the *E. limosum* genome, one of the model acetogenic species, where all genes were targeted for transcriptional suppression. We investigated the fitness contributions of 96% of the total genes identified, revealing the gene fitness and essentiality for heterotrophic and autotrophic metabolisms. Our data show that the Wood–Ljungdahl pathway, membrane regeneration, membrane protein biosynthesis, and butyrate synthesis are essential for autotrophic acetogenesis in *E. limosum*. Furthermore, we discovered genes that are repression targets that unbiasedly increased autotrophic growth rates fourfold and acetoin production 1.5-fold compared to the wild-type strain under CO_2-H_2 conditions. These results provide insight for understanding acetogenic metabolism and genome engineering in acetogenic bacteria.

acetogenic bacteria | Wood–Ljungdahl pathway | CRISPRi screen | autotrophic growth | gas fermentation

Significance

Acetogenic bacteria can fix approximately 20% of the atmosphere's carbon and reduce C1 feedstocks, such as CO_2 or CO, to multicarbon compounds via the Wood–Ljungdahl pathway, thus playing a prominent role in the global carbon cycle. Using a CRISPR interference (CRISPRi) screen, we measured gene fitness at the genome level under heterotrophic and autotrophic growth conditions and demonstrated a strategy to increase the autotrophic growth rate on the basis of this dataset. Our findings can contribute to advancing the understanding of acetogenesis metabolism and further engineering a cell factory system for the sustainable production of value-added chemicals from industrial waste gases.

Acetogenic bacteria are model organisms for converting carbon dioxide (CO_2) into acetate using the Wood–Ljungdahl (W–L) pathway (1), which is the most efficient metabolic pathway for carbon fixation requiring a minimal thermodynamic gradient to produce acetyl-CoA in bacteria (2). In addition to their ecological importance (3), acetogenic bacteria have been used for biotechnological applications, while their metabolic pathways have been engineered to produce multicarbon chemicals from industrial synthesis gas (syngas) through gas fermentation (4, 5). Among acetogenic bacteria, *Eubacterium limosum* can grow autotrophically using syngas, carbon monoxide (CO), or CO_2 with hydrogen (H_2) to form butyrate and acetate (6–8).

Acetogenic bacteria have been well investigated at the system level, revealing their genome sequences, transcription start sites, transcriptomes, translatomes, and proteomes (8–10). Although several key factors of acetogenesis have been well studied (1), significant gaps remain in our knowledge regarding the roles of other genes in heterotrophic and autotrophic acetogenesis (11). Thus, genetic screening methods are required to elucidate the genetic basis for autotrophic phenotypes at the genome scale. Recent advances in programming the CRISPR-Cas system have paved the way for interrogating gene functions through transcriptional interference (CRISPRi) at the genome scale (12). By synthesizing pooled single-guide RNAs (sgRNAs) in array-based oligonucleotide pools, CRISPRi screening has been applied to investigate the fitness of individual genes by calculating the enrichment or depletion in sgRNA levels during cell growth using next-generation sequencing. Because gene fitness is a good metric for evaluating gene essentiality, CRISPRi screening has been used in *Escherichia coli* and other bacterial species (13–18). However, CRISPRi screening is yet to be applied in acetogenic bacteria because the practical size of the genome-scale knockdown library that could be generated under anaerobic conditions was restricted by the inefficiency of plasmid delivery into the acetogens. Recently, gene essentiality of *Clostridium autoethanogenum* was determined using high-throughput random transposon insertion sequencing (TIS). The study showed that the W–L pathway, the Rnf complex, and Nfn are essential for autotrophic growth (19). However, there are limitations to comparing heterotrophic and autotrophic specific gene sets.

Here, we report genome-scale CRISPRi screening using 41,939 sgRNAs designed to target all predicted genes of *E. limosum* ATCC 8486. To investigate its genotype–phenotype

Author contributions: J.S., S.C., and B.-K.C. designed research; J.S., J.B., H.L., S.K., S.J., and Y.S. performed research; J.S. contributed new reagents/analytic tools; J.S., J.B., Y.S., S.C., and B.-K.C. analyzed data; and J.S., J.B., S.C., and B.-K.C. wrote the paper.

The authors declare no competing interest.

This article is a PNAS Direct Submission.

[1]J.S. and J.B. contributed equally to this work.

[2]To whom correspondence may be addressed. Email: bcho@kaist.ac.kr.

This article contains supporting information online at https://www.pnas.org/lookup/suppl/doi:10.1073/pnas.2216244120/-/DCSupplemental.

Published January 30, 2023.

relationships under heterotrophic and autotrophic growth conditions, we generated a CRISPRi library in *E. limosum* using the designed sgRNA library. Based on the abundance of the individual sgRNAs, fitness scores for genes were estimated during cell growth under heterotrophic (glucose) and autotrophic (CO_2-H_2 and syngas) growth conditions. The results revealed that the genes involved in the W–L pathway contribute to both heterotrophic and autotrophic growth. Membrane regeneration, membrane protein biosynthesis, and butyrate synthesis are essential under autotrophic growth conditions. Notably, our CRISPRi data revealed 22 genes with increased autotrophic growth rates after transcriptional repression. We validated that simultaneous inhibition of the expression of three candidate genes significantly enhanced volumetric productivity and autotrophic growth rate. These results provide insight into how acetogenic metabolism can be engineered in an unbiased manner to enhance the autotrophic growth of acetogenic bacteria.

Results

Construction of a Genome-Wide sgRNA Library in *E. limosum*. Acetogenic bacteria are metabolically flexible (20), showing heterotrophic growth when provided organic carbons (e.g., sugars and alcohols) and autolithotrophic growth on C1 gaseous substrates (e.g., CO and CO_2-H_2) (1, 21). To discover 1) the difference in gene essentiality under heterotrophic and autotrophic growth conditions and 2) transcriptional repression targets that increase the autotrophic growth rates, we conducted genome-scale CRISPRi screening in *E. limosum*. First, we created a tiling sgRNA library to repress each gene in *E. limosum* (Fig. 1*A*). Among the 170,691 sgRNAs predicted to have the least off-target effects (22), 39,939 gene-targeting sgRNAs (GT_sgRNA) were selected to target the nontemplate strand proximal to the coding region of 4,130 genes, with one sgRNA per 100 bp of the gene body for 96% coverage of the total genes (Dataset S1). An additional

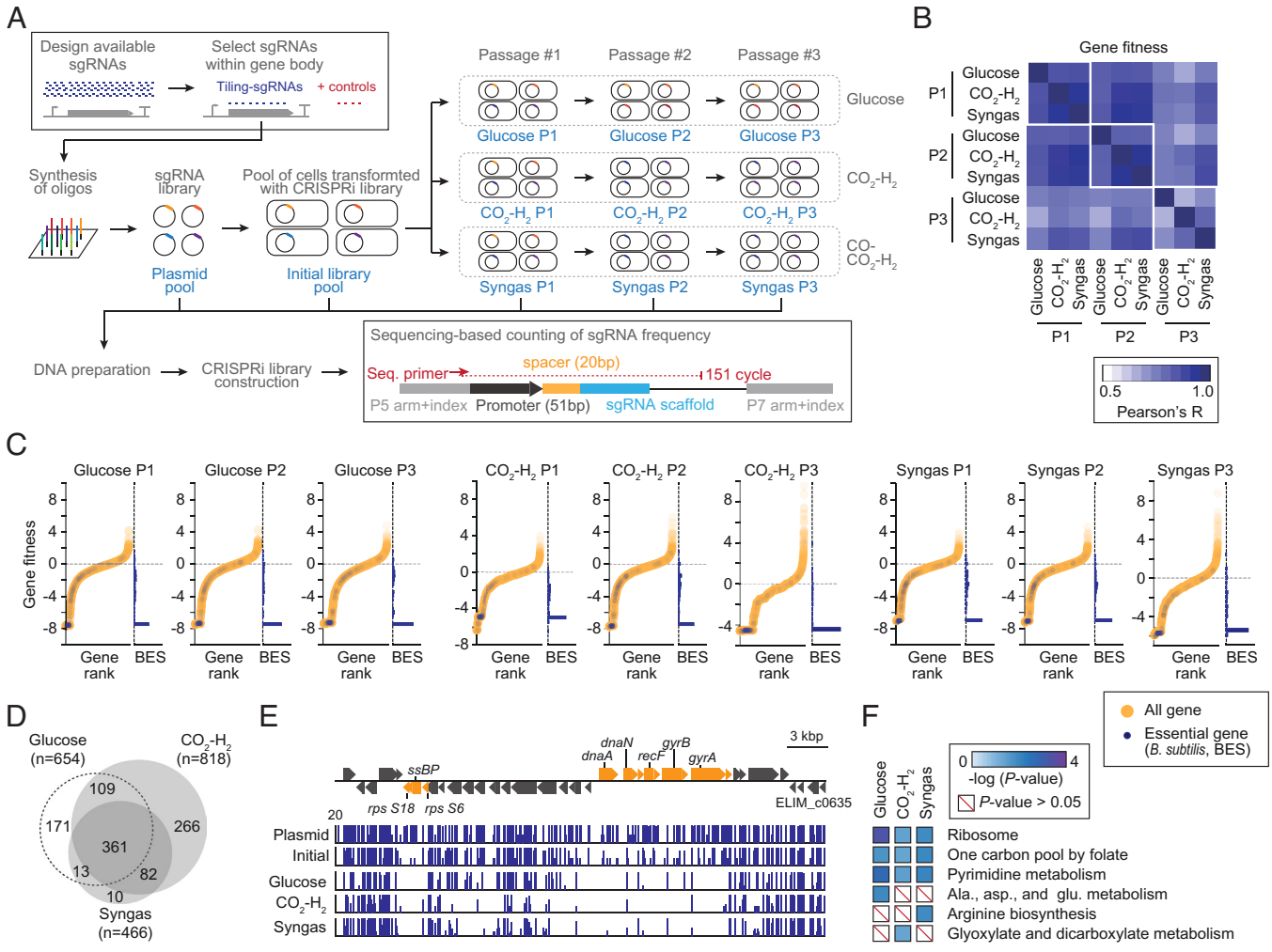

Fig. 1. Genome-scale CRISPRi screening revealing gene fitness under glucose, CO_2-H_2, and syngas growth conditions in *E. limosum*. (*A*) Schematic overview for CRISPRi screening in *E. limosum*. Previously, 170,691 sgRNAs with the least off-target effects were designed for the genome of *E. limosum* (22). Based on the high-efficient sgRNA candidates, we designed a tiling CRISPRi library for the repression of each annotated gene. Oligonucleotides of the sgRNA library were synthesized on a DNA microarray and cloned into an anhydrotetracycline-inducible pJIR-dCas9 vector (22). The plasmid library was then transformed into *E. limosum* to create the cell libraries screened under glucose, CO_2-H_2, and syngas growth conditions. Samples were run in triplicate and sequenced. NGS libraries were generated using the extracted plasmids to determine the change in each sgRNA between the selective and control conditions. (*B*) Heatmap of Pearson's correlation coefficient matrix for the gene fitness scores. Abbreviations: P1, passage 1; P2, passage 2; P3, passage 3. (*C*) All 3,953 genes were ranked by their selective gene fitness. Blue dots represent the 152 homologous genes predicted based on the set of essential genes in *Bacillus subtilis* (BES) (23). Gene densities of BES according to gene fitness are indicated with a blue bar. Mapping of all *E. limosum* genes to BES was conducted using BLAST ($E < 10^{-30}$). (*D*) Comparison of conditionally essential genes identified under glucose, CO_2-H_2, and syngas growth conditions at the P3 stage (*SI Appendix*, Fig. S5). (*E*) Example of sgRNA profiles of the DNA replication system (ELIM_c0624–ELIM_c0629) and small subunit ribosomal protein (S18 and S6, ELIM_c0608–ELIM_c0610). (*F*) KEGG pathway enrichment of essential genes identified from each growth condition at the P3 stage (Benjamini–Hochberg–corrected *P* value < 0.05).

2,000 nontargeting sgRNAs (NT_sgRNA) were also designed for negative controls (5% of total sgRNAs). Oligonucleotides for a total of 41,939 sgRNA sequences were synthesized and cloned into an anhydrotetracycline-inducible pJIR-dCas9 shuttle vector (22) in *E. coli*, and sgRNAs were cloned into an average of 36 unique cells (1.5×10^6 colonies were obtained from a total of 100 parallel transformations; 36-fold coverage). This plasmid pool was transformed into *E. limosum* under anaerobic conditions (*SI Appendix*, Fig. S1*A*), resulting in CRISPRi cell libraries where each plasmid, which included sgRNA and dCas9, was transformed into 150 unique cells (0.6×10^7 colonies were obtained from a total of 600 parallel transformations; 150-fold coverage).

To explore the genetic requirements that contribute to autotrophic growth, we conducted CRISPRi screening under heterotrophic (glucose [N_2, 200 kPa]), autotrophic (CO_2-H_2 [CO_2:H_2 = 20:80; 200 kPa]), and syngas (CO_2-CO-H_2 [CO_2:CO:H_2 = 20:20:60; 200 kPa]) growth conditions (*SI Appendix*, Fig. S1*B*). These cultures were grown to an OD_{600} of ~0.3 at 37 °C, with three biological replicates to achieve approximately three doubling growths for each experiment. The abundance of each sgRNA was determined using next-generation sequencing (*SI Appendix*, Fig. S1*C*), which resulted in 1,575 NT_sgRNAs (5% of total sgRNAs) and 29,957 GT_sgRNAs (95% of total sgRNAs) that targeted 4,102 genes in the CRISPRi libraries (Dataset S2 and *SI Appendix*, Fig. S1*D*). As cultures progressed under the growth conditions (P1 to P3; up to 10 doublings), we observed that the difference in sgRNA levels gradually increased (*SI Appendix*, Fig. S1*E*) from P1 (coefficient of variation $[CV]_{glucose}$ = 160%, $CV_{CO2\text{-}H2}$ = 145%, and CV_{syngas} = 140%) to P3 ($CV_{glucose}$ = 205%, $CV_{CO2\text{-}H2}$ = 2,438%, and CV_{syngas} = 3,432%), indicating the enrichment or depletion of GT_sgRNAs. The consistency of the mapping ratio of NT_sgRNAs (*SI Appendix*, Fig. S1*F*) and differential clustering of glucose, CO_2-H_2, and syngas samples through visualization of principal coordinate analysis (*SI Appendix*, Fig. S1*G*) confirmed the reliability of these experiments. Using the dataset generated by CRISPRi screening under all conditions, we investigated the influence of the sgRNA position within the gene body on their activities. We classified all sgRNAs into subgroups based on their relative location along the gene body and found that there was no statistical difference in sgRNA activity according to the location of the sgRNAs (*SI Appendix*, Fig. S1*H*) similar to observations reported for *E. coli* (18).

Determination of Gene Fitness and Essentiality under Autolithotrophic Growth Conditions. First, we estimated the fitness effect of the sgRNAs under each growth condition. The fitness scores of sgRNAs (Z_{sgRNA}) under glucose, CO_2-H_2, and syngas growth conditions were calculated by their enrichment or depletion compared to Z-scores of the plasmid library (13, 24) (Dataset S3). Gene fitness was determined by grouping the Z_{sgRNAs} of their target genes (13) using the 95th percentile of the Z-scores of gRNAs. To better quantify the fitness of each gene while avoiding sgRNAs with potential off-target effects, we compared five alternative metrics (*Materials and Methods*) and chose P_{75}-Z (e.g., the 75th percentile of the Z-score of sgRNAs) to represent the fitness effects of the genes, with the goal of quantifying both the negative (i.e., depletion of sgRNAs) and positive (i.e., enrichment of sgRNAs) fitness effects (Dataset S4). The P_{75}-Z metric showed good correlation with the fold change of the raw reads (*SI Appendix*, Fig. S2*A*) and high reproducibility within the biological replicates (median Pearson's r = 0.85) (*SI Appendix*, Fig. S2*B*), indicating the robustness of this method. As the culture passage progressed, Pearson's correlation coefficient matrix of the gene fitness scores became more different between the glucose and CO_2-H_2 conditions (0.86 in P1, 0.82 in P2, and 0.64 in P3) than between the CO_2-H_2 and syngas conditions (0.95 in P1, 0.95 in P2, and 0.82 in P3) (Fig. 1*B*), suggesting that both autotrophic growth conditions showed similar global gene fitness characteristics.

Next, we defined the essential genes under a given condition when the gene fitness was lower than the essentiality threshold by fitting the distribution of gene fitness with a gaussian curve, while the remaining curves were defined as essential genes (*SI Appendix*, Fig. S3*A*). We observed a significant reduction in the abundance of sgRNAs that targeted the 152 homologous genes predicted based on the set of essential genes in *B. subtilis* (BES) (25) (Fig. 1*C*). These results indicated that the sgRNA level could be used as a proxy for gene fitness in pooled competitive growth. The most essential genes (95%) under the syngas condition extensively overlapped with essential genes under CO_2-H_2 conditions, but only 71% of the essential genes under glucose conditions were identical to those identified under CO_2-H_2 conditions (Fig. 1*D*). Furthermore, we defined 361 genes as "core essential genes" that were required for heterotrophic and autotrophic growth (Fig. 1*D* and Dataset S4). This number is close to the 404 and 439 essential genes reported in *Clostridium difficile* (26) and *C. autoethanogenum* (19), respectively. For example, ribosomal, chaperone, aminoacyl-tRNA biosynthesis, and DNA replication proteins were included in the core essential genes and consistent with gene essentiality in *E. coli* (27) (Fig. 1*E* and *SI Appendix*, Figs. S4 and S5). We then examined the overall classification of the core essential genes identified in the CRISPRi screen. Kyoto Encyclopedia of Genes and Genomes (KEGG) enrichment analysis showed that putative essential genes were mainly related to genetic translation, pyrimidine metabolism, and amino acid metabolism (Fig. 1*F* and *SI Appendix*, Fig. S3*B*). Interestingly, core essential genes were statistically enriched for "one carbon pool by folate" under all growth conditions, suggesting that carbon fixation pathways in prokaryote-related genes were essential under all growth conditions (*SI Appendix*, Fig. S4).

Genes with Condition-Dependent Fitness during Heterotrophic and Autotrophic Growth. Next, we identified specific genes that were essential for cell growth under each condition to provide insights into autotrophic growth of acetogenic bacteria. A total of 1,618 genes (40.9%) showed significant changes in gene fitness ($P < 0.05$, Mann–Whitney U test) under at least one condition, suggesting these genes contribute to fitness under heterotrophic and autotrophic growth conditions (Fig. 2*A*). Genes were grouped into 15 clusters based on their depletion or enrichment levels by performing unsupervised K-means clustering analysis (*SI Appendix*, Fig. S6*A*). Among these clusters, we found three with genes that were highly enriched or depleted under autotrophic growth conditions. Interestingly, cluster I (22 genes) had genes that were gradually enriched under CO_2-H_2 and syngas conditions, revealing an increase in autotrophic growth rates when the expression of these genes is repressed (*SI Appendix*, Fig. S6*A*). In contrast, clusters VIII (95 genes) and IX (51 genes) were enriched with genes that were gradually depleted under CO_2-H_2 and syngas conditions (*SI Appendix*, Fig. S6 *B* and *C*). Clusters II, V, VII, and X contained 341 genes that were highly depleted under all growth conditions tested (Fig. 2*A*). Gene ontology (GO) and KEGG enrichment analyses showed that these four clusters were significantly enriched in essential genes involved in fundamental biological processes (Benjamini–Hochberg–corrected $P < 0.05$), such as DNA replication, cell division, translation, transcription, and one-carbon metabolic processes (e.g., one carbon pool by folate), with cluster V containing acetogenesis-related genes (Fig. 2*B*) and cluster VII containing genes in cellular amino acid metabolic processes. Among all the amino acid biosynthesis

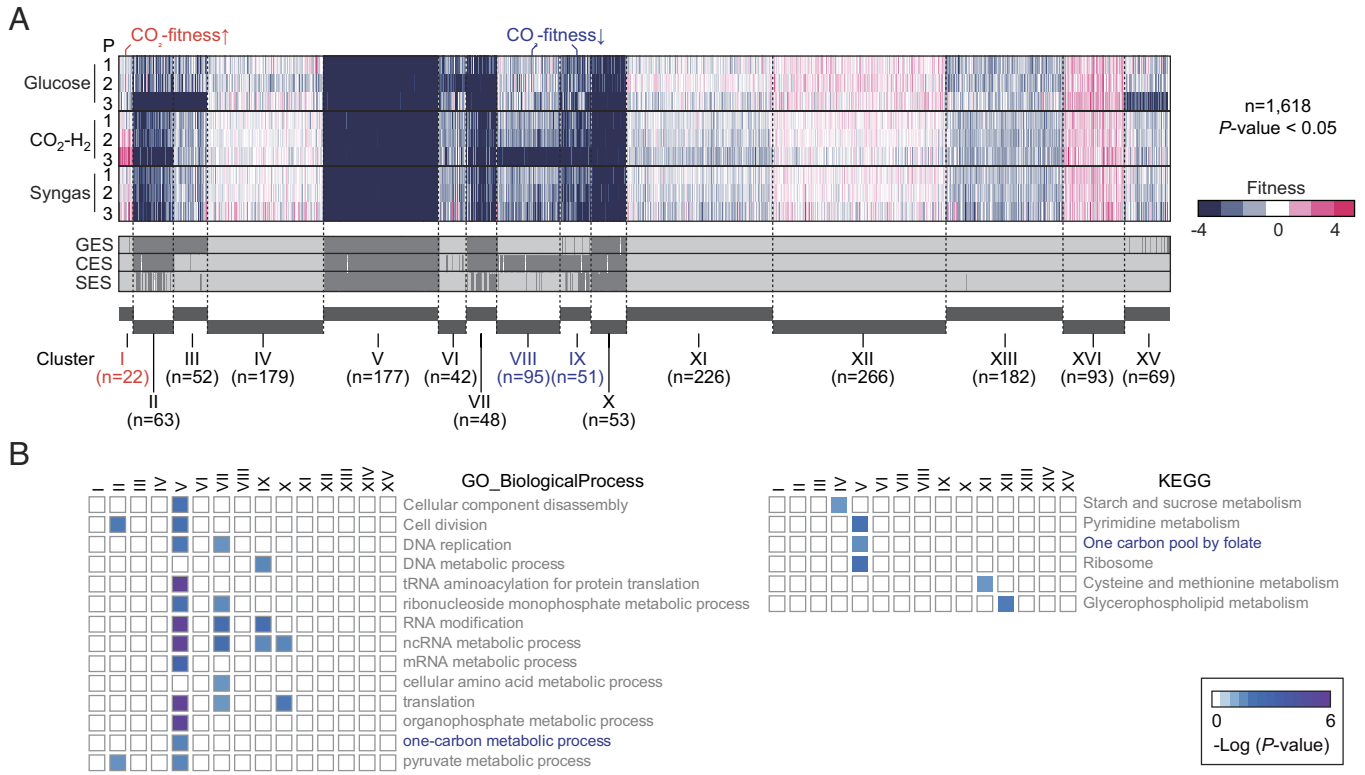

Fig. 2. Dynamics of global gene fitness during heterotrophic and autotrophic growth in *E. limosum*. (*A*) Heatmaps of the genes clustered by similarity of fitness change over time under glucose, CO_2-H_2, and syngas growth conditions. The heatmap shows the fitness values (from red to blue) for each passage (P1 to P3). Abbreviations: GES, the set of essential genes under the glucose growth condition; CES, the set of the essential genes under the CO_2-H_2 growth conditions; and SES, the set of the essential genes under the syngas growth condition. (*B*) Enriched GO terms and KEGG pathways for all gene clusters. A Benjamini–Hochberg–corrected $P < 0.05$ was considered significant.

pathways, we identified alanine, serine, glutamine, and methionine biosynthesis pathways that were essential under all growth conditions (*SI Appendix*, Fig. S7).

W–L Pathway Plays an Important Role in Heterotrophic Growth of Acetogenic Bacteria. We investigated how the fitness of acetogenesis-associated genes changed under the growth conditions tested (Fig. 3*A*). Consistent with the GO and KEGG enrichment analyses (Figs. 1*F* and 2*B*), sgRNAs that targeted acetogenesis-related genes, including those that encode formate dehydrogenase, the W–L pathway, hydrogenase, the Rnf complex, and adenosine 5′-triphosphate (ATP) synthase, were depleted under all growth conditions as the passage progressed from P1 to P3 (*SI Appendix*, Fig. S8). Among them, genes encoding methyl branch, carbonyl branch, phosphotransacetylase, and acetate kinase were essential, even under glucose conditions (Fig. 3*A*). These findings were consistent with the high translation level of hydrogenase, the Rnf complex, ATP synthase, and the W–L pathway under glucose conditions, as previously reported (8, 9). To confirm heterotrophic growth repression, we constructed two CRISPRi mutants (Fig. 3*B*), *folD* and *acsB*. The growth rate and maximum biomass (OD_{600}) of *folD* in the methyl-branch and *acsB* in the carbonyl-branch mutants were significantly decreased under heterotrophic (growth rate, 0.74- to 0.80-fold decrease, $P < 0.018$; maximum biomass, 0.49- to 0.67-fold decrease, $P < 0.004$) and autotrophic growth conditions (growth rate, 0.18- to 0.20-fold decrease, $P < 0.003$; maximum biomass, 0.64- to 0.67-fold decrease, $P < 0.008$). These data indicated that the W–L pathway significantly contributes to the heterotrophic growth of *E. limosum*.

Furthermore, we investigated the fitness of genes involved in central carbon metabolism under heterotrophic and autotrophic growth conditions (*SI Appendix*, Fig. S9). Interestingly, genes related to glycolytic/gluconeogenesis, except for glucokinase, fructose 1,6-bisphosphate aldolase, and enolase, were essential under both heterotrophic and autotrophic growth conditions. Overall, the gene fitness of the important carbon metabolism pathways, including the W–L pathway, did not differ significantly between autotrophic and heterotrophic growth conditions when organic carbon was used.

Genes Involved in Membrane Regeneration and Membrane Protein Biogenesis That Are Essential for Autotrophic Growth. To examine the genetic basis for the differences in gene fitness between heterotrophic and autotrophic growth conditions, we focused on the genes in clusters VIII (n = 95) and IX (n = 51), whose knockdown induced a significant growth defect under CO_2-H_2 (cluster VIII) and syngas (clusters VIII and IX) growth conditions (Fig. 4*A*). Cluster VIII includes the major genes in the phosphatidic acid formation process for membrane regeneration (Fig. 4 *B* and *C*), indicating that gene fitness for fatty acid biosynthesis was significantly decreased when compared with heterotrophic growth conditions ($P < 0.01$, Mann–Whitney U test) (*SI Appendix*, Fig. S4). In *E. coli*, phosphatidic acid biosynthesis is regulated by the acyl-acyl carrier protein (acyl-ACP) formed from fatty acid elongation, which inhibited acetyl-CoA carboxylase (ACC), enoyl-(acyl-carrier-protein) reductase II (FabK), and 3-oxoacyl-[acyl-carrier-protein] synthase 3 (FabH) and is dependent on the long-chain acyl-ACP (16 to 18 carbon) concentration (28). These results suggested that long acyl-ACP concentration during phosphatidic acid biosynthesis was insufficient under autotrophic growth conditions.

In addition, we found that the essential genes in cluster IX were specifically related to the protein secretion system. SecDF, which

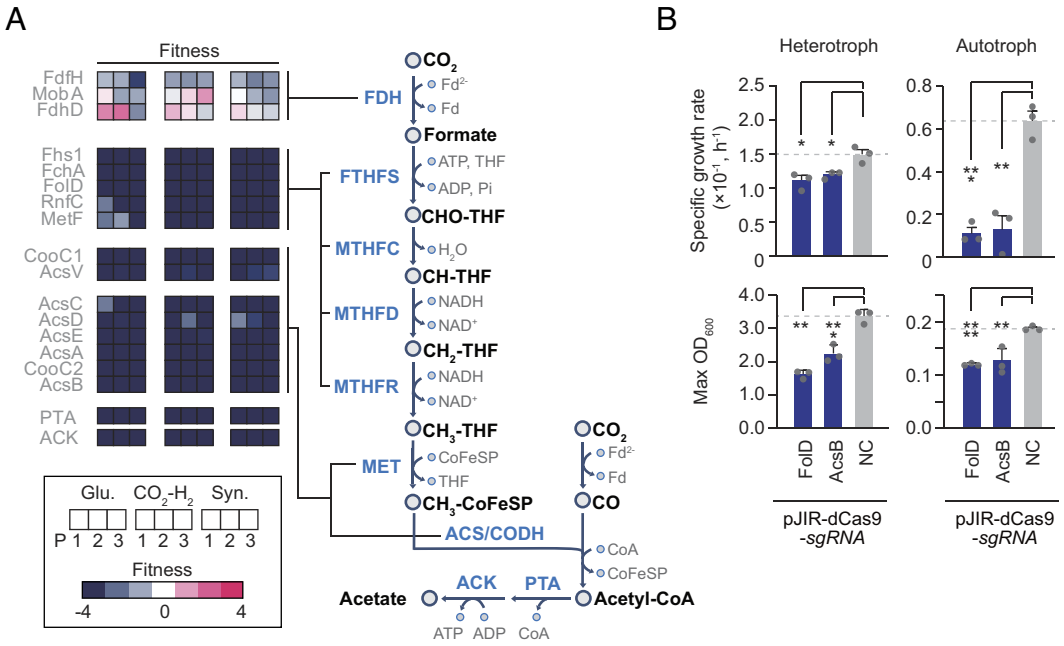

Fig. 3. Gene fitness of the W–L pathway during heterotrophic and autotrophic growth in *E. limosum*. (*A*) The heatmap shows the fitness value (red to blue) for each passage (P1 to P3) under glucose and CO_2-H_2 growth conditions. Abbreviations: FDH, formate dehydrogenase; FTHFS, formyl-THF synthetase; MTHFS, formyl-THF cyclohydrolase; MTHFD, methylene-THF dehydrogenase; MTHFR, methylene-THF reductase; MET, methyltransferase/corrinoid iron–sulfur protein; ACS/CODH, acetyl-CoA synthase/CO dehydrogenase; PTA, phosphotransacetylase; ACK, acetate kinase. (*B*) The specific growth rate of two W–L pathway knockdown strains treated with 30 ng/mL anhydrotetracycline cultured under glucose (heterotrophic) or CO_2-H_2 (autotrophic) growth conditions (n = 3, independent biological replicates). Significance was assessed by comparing the control strain that contained NT_sgRNA (NC) and the mutants that contained sgRNAs targeting *folD* (ELIM_c0959) and *acsB* genes (ELIM_c1655), which are involved in the methyl branch and carbonyl branch of the W–L pathway, respectively, using Student's *t* test (ns, not significant; *P < 0.05; **P < 0.01; ***P < 0.001; ****P < 0.0001).

is part of the Sec protein translocase complex, uses an additional proton motive force in *E. coli* (or a sodium motive force that depends on the species, e.g., *Vibrio* spp.) to move secretory proteins through the SecA and SecYEG core complex (29) (Fig. 4*D*). They were also involved in membrane protein insertion through complex formation with SecYEG and the insertase YidC (30). Unlike SecA and SecYEG, which were essential under all growth conditions tested, *secD* and *secF* had very low gene fitness under autotrophic growth conditions (Fig. 4*D*), indicating that membrane protein insertion and sodium motive force–driven protein secretion were essential under these conditions. To confirm the gene fitness of phosphatidic acid biosynthesis and the SecDF complex, we constructed two CRISPRi mutants containing sgRNAs that targeted the *secD* gene in the *secDF* operon (ELIM_c1731–ELIM_c1732) or the *accB* gene in the *accABCD* operon (ELIM_c2957–ELIM_c2960), respectively (Fig. 4*E*). The growth rates and maximum OD_{600} of *secD* (growth rate, 0.25-fold decrease, P = 0.027; maximum OD_{600}, 0.76-fold decrease, P = 0.002) and *accB* (0.17-fold decrease, P = 0.012; max OD_{600}, 0.73-fold decrease, P = 0.008) mutants were significantly lower under autotrophic growth conditions than those under heterotrophic growth conditions.

We also investigated the fitness of membrane proteins that may play a role in establishing a sodium ion potential in redox balancing and ATP generation during acetogenesis. Under all growth conditions tested, we observed that the repression of genes encoding membrane proteins was beneficial for cell growth (P < 0.001, Mann–Whitney U test). As the number of transmembrane domains (TMs) of the protein increased, its fitness significantly increased (P < 0.01, Mann–Whitney U test) under CO_2-H_2 and syngas conditions, indicating that repression of transporter/channel proteins with a high number of TMs can provide an energetic advantage to autotrophic growth. Taken together, de novo formation of membrane lipids and protein complexes associated with membrane protein insertion/secretion was essential to cell growth under autotrophic conditions, indicating that inhibition of membrane proteins with a high number of TM is beneficial during autotrophic growth.

Electron Bifurcation EtfAB–BCD Complex Is Selectively Essential under High H_2 Conditions. Interestingly, the butyrate biosynthesis–related genes, not related to acetogenesis or autotrophic growth, were found in clusters VIII and IX (Fig. 5*A*). Among these genes, butyryl-CoA dehydrogenase (BCD, ELIM_c0231) was found to be essential under all tested growth conditions. We attempted to perform CRISPRi-based knockdown and CRISPR/Cas9-based knockout of the BCD gene on DSMZ medium 135 and RCM agar plates, respectively, more than three times, but an appropriate mutant could not be obtained during the study. Genes required for the synthesis of butanoyl-CoA, including those that encode acetyl-CoA acetyltransferase, 3-hydroxybutyryl-CoA dehydrogenase, 3-hydroxybutyryl-CoA dehydratase (CRT), and the BCD–Etf complex, were all essential under CO_2-H_2 growth conditions. Electron transfer flavoproteins present in the BCD operon (ELIM_c0229–ELIM_c0234) form the BCD–Etf complex that can bifurcate (31) and convert two nicotinamide adenine dinucleotides (NADHs) into Fd^{2-}. This bifurcating system is the only one for the reduction of ferredoxin (E0 = −420 mV) with NADH (−320 mV) in *E. limosum* (31). The resulting reduced ferredoxin is thought to be oxidized by the Rnf complex to generate a sodium gradient, while ATP is generated by F_1F_0 ATP synthase. Under CO_2-H_2 conditions (CO_2:H_2 = 20:80), the oxidation of 8 moles H_2 was coupled to the reduction of 4 moles NAD+ and 4 moles ferredoxin, with the reducing equivalents and 4 moles CO_2 incorporated into the W–L pathway to form 2 moles acetate, which results in 8 moles H_2, whose oxidation can generate

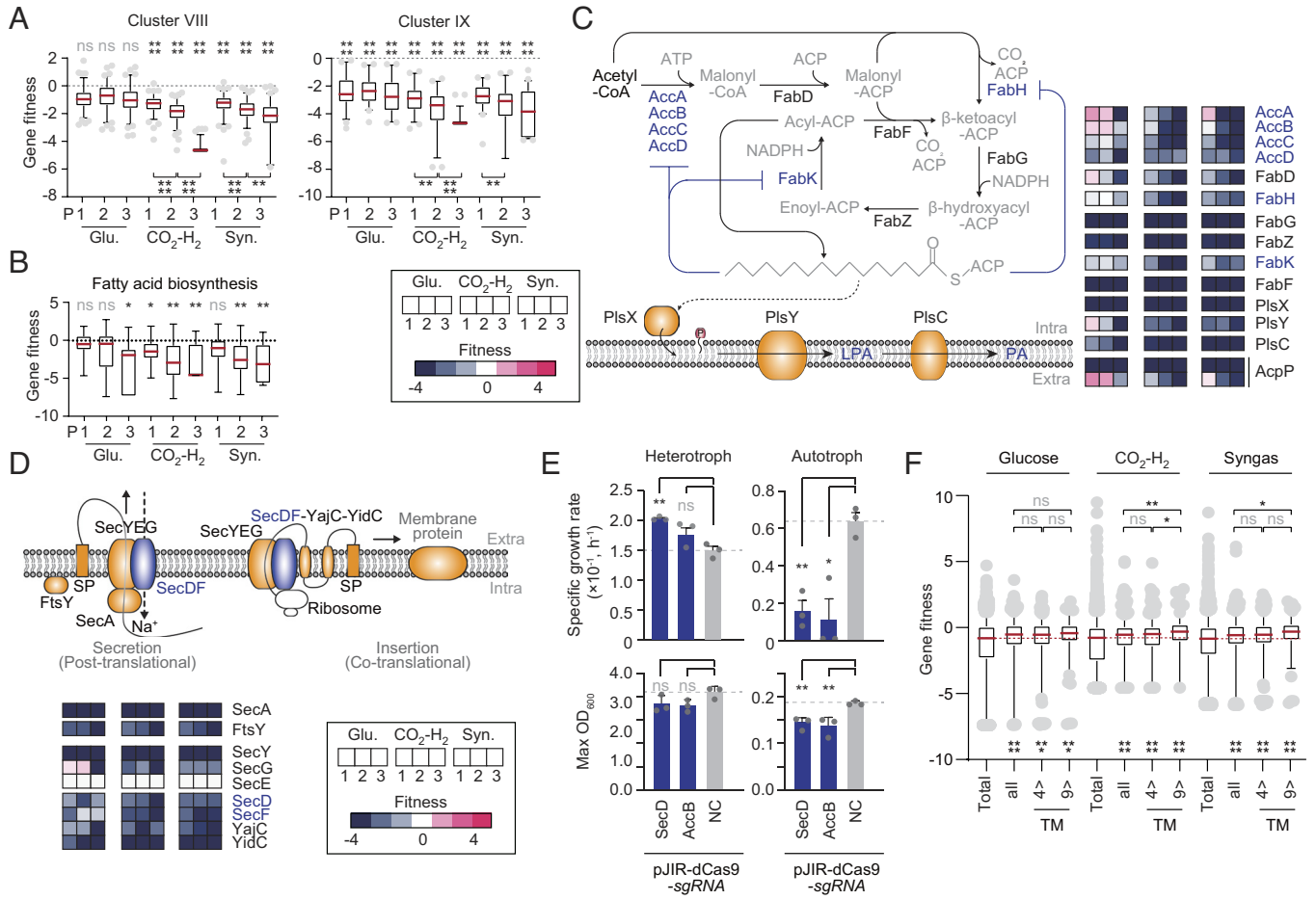

Fig. 4. Condition-dependent low-fitness genes in *E. limosum* under autotrophic growth conditions. (*A*) Gene fitness comparison of clusters VIII and IX under glucose, CO_2-H_2, and syngas growth conditions. Symbols located above each plot indicate significance between total genes and those in each cluster for each passage (P1 to P3). Significance was assessed by the Mann–Whitney U test (ns, not significant; *P < 0.05; **P < 0.01; ***P < 0.001; ****P < 0.0001). (*B*) Gene fitness of fatty acid biosynthesis–related genes under glucose, CO_2-H_2, and syngas growth conditions. Symbols indicate significance between total genes and those involved in fatty acid biosynthesis for each passage (P1 to P3). Significance was assessed by the Mann–Whitney U test (ns, not significant; *P < 0.05; **). (*C*) Gene fitness of the major genes in the phosphatidic acid formation process during membrane regeneration. The heatmap shows the fitness values (red to blue) for each passage (P1 to P3). (*D*) Gene fitness of SecYEG and SecDF-YajC-YidC holotranslocon protein secretase/insertase. The heatmap shows the fitness values (red to blue) for each passage (P1 to P3). (*E*) The specific growth rates of SecDF and AccABCD operon knockdown strains treated with 30 ng/mL anhydrotetracycline and grown in glucose or CO_2-H_2 conditions (n = 3, independent biological replicates). Significance was assessed by comparing the control strain (nontargeting sgRNA, NC) and the mutants expressing sgRNAs targeting *secD* (ELIM_c1731) and *accB* (ELIM_c2957), which are involved in *secDF* (ELIM_c1731–ELIM_c1732) and *accABCD* (ELIM_c2957 ELIM_c2960) operons using Student's *t* test (ns, not significant; *P < 0.05; **P < 0.01). (*F*) Gene fitness distribution across the number of transmembrane domains in target membrane proteins. Symbols located below each plot indicate significance between the total genes and the genes of membrane proteins under glucose, H_2-CO_2, and syngas growth conditions. Significance was assessed with the Mann–Whitney U test (ns, not significant; *P < 0.05; **P < 0.01; ***P < 0.001; ****P < 0.0001). To analyze the gene fitness of obligate transmembrane protein members, we generated a list of transmembrane proteins with predicted or known topologies based on the UniProt database.

4 moles reduced ferredoxin and NADH, during acetogenesis. If all three NADHs and one acetate are used for butyrate biosynthesis, one Fd^{2-} and one acetyl-CoA can be produced. Therefore, because a total of two Fd^{2-} can be converted to one ATP and two NADHs through the Rnf complex and acetyl-CoA can be converted to one ATP and one acetate, the BCD reaction can act as an additional ATP generation pathway (Fig. 5*A*). In contrast, under syngas conditions (CO_2:CO:H_2 = 20:20:60), H_2 did not have such an advantage because all reducing equivalents generated from H_2 were incorporated into the acetogenesis reaction; therefore, the fitness of the butyrate biosynthesis pathway was relatively low compared to that of CO_2-H_2. Under gaseous conditions such as CO_2 or CO, butyrate was only produced in bioreactors under high CO partial pressure conditions in the *E. limosum* KIST612 strain (32). Also, addition of 30 mM sodium acetate to the medium greatly enhanced butyrate production (33). Although CO conditions are energetically more favorable for butyrate production (3.5 mol ATP/mol butyrate), butyrate production through the electron-bifurcating BCD under H_2-CO_2 conditions (1 mol ATP/mol butyrate) is theoretically possible (31). To confirm whether the BCD–EtfAB reaction occurs under H_2-CO_2 conditions, we conducted a bioreactor experiment (Fig. 5*B*). When acetate reached approximately 2.2 g/L (36 mM), butyrate formation was observed. Finally, we observed that 0.708 g/L (8 mM) butyrate was formed after approximately 356 h of fermentation under CO_2-H_2 growth conditions. These data suggested that the butyrate biosynthesis pathway plays an important role in the redox balance and ATP generation under high H_2 conditions.

Genes Involved in DNA Repair Systems and Protein Chaperones Are Essential under Autotrophic Growth Conditions. Among the genes in clusters VIII and IX, additional genes involved in the DNA repair system and chaperone proteins were also identified (*SI Appendix*, Fig. S10). In the DNA repair system, the MutL/MutS, the SbcCD complex, RecJ, SSBP, and RecA were essential under CO_2-H_2 and syngas growth conditions but not under

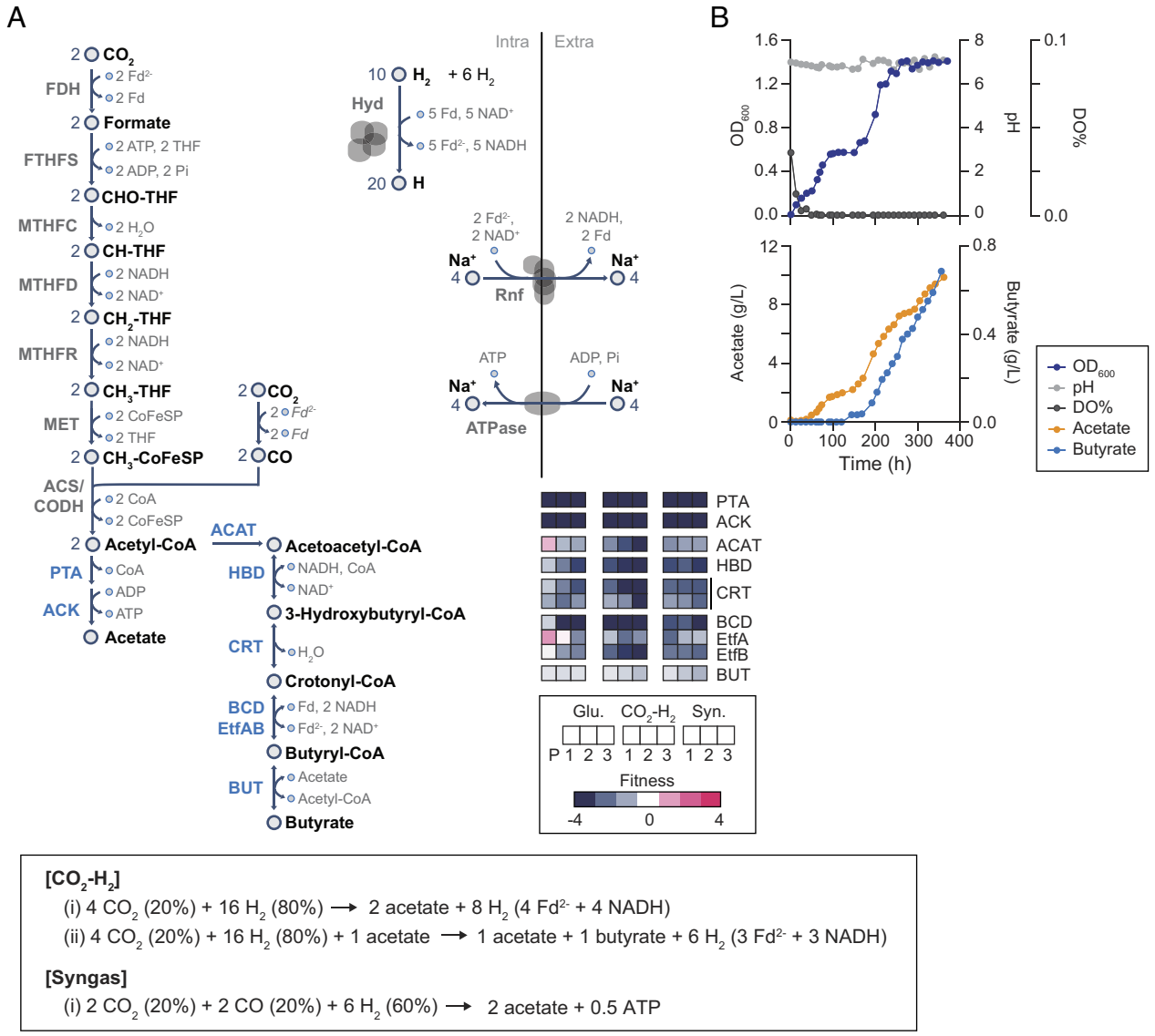

Fig. 5. Gene fitness of acetate and butyrate biosynthetic pathways during heterotrophic and autotrophic growth of *E. limosum*. (*A*) Fitness of genes involved in the biosynthesis pathways for acetate and butyrate (ELIM_c0229–ELIM_c0234). The heatmap shows the fitness values (from red to blue) for each passage (P1 to P3). Two types of overall reactions, (i) and (ii), are predicted under CO_2-H_2 or syngas growth conditions. The overall reactions (i) and (ii) showed the production of 2 moles acetate only or the production of 1 mole butyrate from CO_2-H_2 or syngas, respectively. The overall reaction (ii) under the CO_2-H_2 growth conditions is shown as a schematic representation in this panel, indicating the BCD bifurcating reaction (BCD–EtfAB, ELIM_c0229–ELIM_c0231) in *E. limosum*. Under the CO_2-H_2 growth conditions, 10 moles H_2 is converted into 5 moles Fd^{2-} and 5 moles NADH via the bifurcating hydrogenase (Hyd). The oxidation of 8 moles H_2 was coupled to the reduction of 4 moles NAD+ and 4 moles ferredoxin, with the reducing equivalents and 4 moles CO_2 incorporated into the W–L pathway to form 2 moles acetyl-CoA. The BCD bifurcating system can further convert 2 moles NADH into 1 mole Fd^{2-}. Additionally, generating 2 moles Fd^{2-} can generate 2 moles NADH and 1 mole ATP through the Rnf complex and ATPase under CO_2-H_2 growth conditions. One molecule of acetate is converted to acetyl-CoA by butyryl CoA:acetate CoA transferase (BUT, ELIM_c1492). It is then converted back to acetate, producing one molecule of ATP. (*B*) Time profile showing the optical density (OD_{600}), pH, dissolved oxygen (DO), acetate production, and butyrate production during *E. limosum* batch fermentation under the CO_2-H_2 growth conditions in a 1-L bioreactor.

the glucose growth condition (*SI Appendix*, Fig. S10*A*). In the chaperone system, the KJE system (DnaK, DnaJ, and GrpE) was essential under all growth conditions tested, while the ELS system (GroES and GroEL) was essential under CO_2-H_2 and syngas conditions (*SI Appendix*, Fig. S10*B*). Although there are proteins that are dependent on the ELS system, such as MetK (34) and membrane proteins that interact with SecA (35), each system has overlapping functions and participates in protein folding (36). The ESL system also plays a central role in the removal of misassembled or abnormal proteins, responses to stress conditions, and metabolic pathway adjustments through its involvement in proteasome assembly (37). Overexpression of GroESL and DnaK improved the productivity of *Clostridium ljungdahlii* and *C. autoethanogenum*, indicating that a protection system against protein misfolding is essential during autotrophic growth (38, 39). Thus, our data suggested that DNA stability and protein folding are more important under autotrophic growth conditions than under heterotrophic growth conditions.

Improvement of Autotrophic Growth Based on CRISPRi Screening Data. CRISPRi screening in *E. limosum* also identified candidates for enhancing an acetogenesis phenotype. In cluster I, we identified 22 genes that were beneficial for autotrophic growth under CO_2-H_2 or syngas conditions when repressed ($P < 0.05$, Mann–Whitney U test) (Fig. 6*A*). Thus, these genes are potential candidates for targeted repression to improve the acetogenesis phenotype. To confirm autotrophic growth improvement, we selected the top 12 genes with the highest increase in gene fitness and constructed

CRISPRi mutants (Fig. 6*B*). Among them, mutants of ELIM_c2976 (a putative Fe–S binding protein), ELIM_c1759 (a Rho protein), and ELIM_c1868 (a putative transcription regulator) showed significantly higher autotrophic growth rates than the control strain ($P < 0.05$, Student's *t* test). A quantitative RT–PCR assay (Fig. 6*C*) confirmed that these three mutants independently showed almost no expression of each gene when compared to the control (<0.08-fold, $P < 0.0001$, Student's *t* test), demonstrating that their suppression improved the autotrophic growth rate.

The growth rate of the ELIM_c2976 mutant was the highest, resulting in a 1.98-fold increase in growth rate when compared with the wild-type strain ($P = 0.004$, Student's *t* test). The protein encoded by ELIM_c2976 was most similar in sequence to QueG, an epoxyqueuosine reductase that converts epoxyqueuosine to queuosine; however, the epoxyqueuosine reductase domain is poorly conserved (*SI Appendix*, Fig. S11). Identification of the *rho* gene ELIM_c1759 was totally unexpected. NusG, NusB, and NuaA, which are fundamental to transcription termination, appeared to be essential under all growth conditions. However, in the case of Rho, its inhibition was more favorable for cell growth under CO_2-H_2 and syngas growth conditions (*SI Appendix*, Fig. S12*A*).

To elucidate the effects of the repression of the candidate genes (ELIM_c2976, ELIM_c1759, and ELIM_c1868) on global gene expression, we performed RNA-seq using the three CRISPRi mutants (c2976i, c1759i, and c1868i) and a control strain (NCi) under heterotrophic (glucose) and autotrophic (CO_2-H_2) conditions (Dataset S5). The correlation coefficient between the biological replicates demonstrated experimental reproducibility (Pearson's r > 0.984) (*SI Appendix*, Fig. S13*A*). Similar to the results of the quantitative RT–PCR assay (Fig. 6*C*), there was no expression of each target gene (*SI Appendix*, Fig. S13*B*). Interestingly, only the c1868i strain showed a distinct difference in gene expression (Pearson's r < 0.789) from the other mutants under CO_2-H_2 conditions, indicating that the ELIM_c1868 TF globally affects gene expression under these conditions (Fig. 6*D*). We then examined the overall classification of the differentially expressed genes ($\log_2$ |fold change| > 1, adjusted *P* value < 0.01) between each CRISPRi mutant and NCi through GO term enrichment analysis. Transcriptome analysis

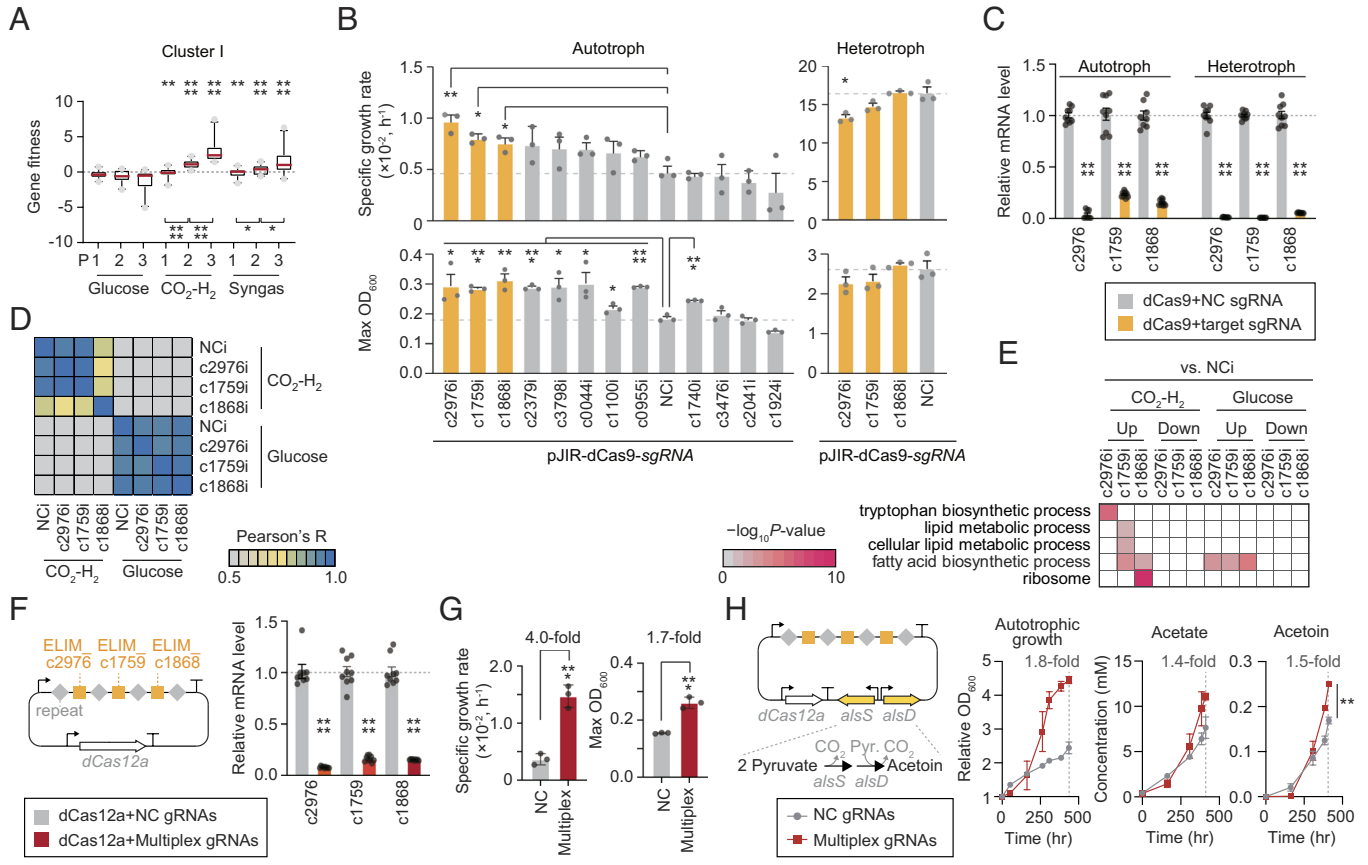

Fig. 6. *E. limosum* mutants with an autotrophic growth advantage. (*A*) Gene fitness comparison of cluster I genes. Symbols located above each plot indicate significant differences between the total genes and those involved in cluster I for each passage (P1 to P3). Significance was assessed with the Mann–Whitney U test (ns, not significant; *$P < 0.05$; **$P < 0.01$; ***$P < 0.001$; ****$P < 0.0001$). (*B*) Specific growth rates and maximum OD_{600} (max OD_{600}) of 12 knockdown strains under CO_2-H_2 growth conditions. Data are presented as means ± SEM from three different biological replicates. Significance was assessed using Student's *t* test (*$P < 0.05$; **$P < 0.01$; ***$P < 0.001$; ****$P < 0.0001$). (*C*) Quantitative RT–PCR analysis. The data are presented as the mean (n = 9) ± SEM. The *gyrA* gene was used as a reference. Significance was assessed using Student's unpaired *t* test (****$P < 0.0001$). (*D*) Pearson's correlation coefficient matrix of gene expression profiles. Each value is shown as a row and column, with the order of growth condition being the same on both axes. (*E*) Enriched GO terms (Benjamini–Hochberg–corrected $P < 0.05$) of differentially expressed genes ($\log_2$ |fold change| > 1, adjusted *P* value < 0.01) from the RNA-seq samples. Full significant differential GO terms are listed in Dataset S6. (*F*) dCas12a-based CRISPRi for the simultaneous repression of ELIM_c2976, ELIM_c1759, and ELIM_c1868 gene expression. *Left* panel: CRISPR array designed for targeting ELIM_c2976, ELIM_c1759, and ELIM_c1868 genes. *Right* panel: Quantitative RT–PCR analysis of ELIM_c2976, ELIM_c1759, and ELIM_c1868 genes in the mutant cells. The data are presented as means (n = 9) ± SEM. The *gyrA* gene was used as a reference. Data are presented as means ± SEM from three different biological replicates. Significance was assessed using Student's unpaired *t* test (***$P < 0.001$; ****$P < 0.0001$). (*G*) Specific growth rates and max OD_{600} of dCas12-based multiplex gene repression mutants (multiplex) and the control (NC) under CO_2-H_2 growth conditions. Data are presented as means ± SEM from three different biological replicates. Significance was assessed using Student's *t* test (***$P < 0.001$). (*H*) Growth profiling and production of acetate and acetoin dCas12-based multiplex gene repression mutants and the control. For acetoin production, a previously validated acetoin biosynthetic pathway (P0077-U1121 for *alsS* and P1121-U1121 for *alsD*) was used to produce high levels of autotrophic acetoin production in *E. limosum* (40). Data are presented as means ± SEM from biological duplicate samples. Significance was assessed using Student's *t* test (**$P < 0.01$).

revealed that the repression of ELIM_c2976 activated the tryptophan operon under CO_2-H_2 growth conditions (log_2 fold changes > 3.12 and $P_{adj} < 0.0005$) (Fig. 6*E* and *SI Appendix*, Fig. S13*C*), suggesting that ELIM_c2976 is involved in tryptophan metabolism. Second, all genes related to fatty acid biosynthesis (except for one *fabG* and one *acpP* gene copy) were significantly up-regulated in c1759i (log_2 fold changes > 1.60 and $P_{adj} < 8.52 \times 10^{-8}$) and c1868i strains ($log_2$ fold changes > 1.56 and $P_{adj} < 5.89 \times 10^{-9}$) under both heterotrophic and autotrophic conditions (Fig. 6*E* and *SI Appendix*, Fig. S13*D*). Consistent with the results of CRISPRi screening, transcriptome analysis also highlighted that the phosphatidic acid biosynthesis pathway was a bottleneck for autotrophic acetogenesis under carbon- and energy-limited CO_2-H_2 conditions. Third, except for RP-L7 and RP-L30, genes encoding ribosomal proteins were significantly increased in the c1868i strain (log_2 fold changes > 0.46 and $P_{adj} < 0.05$) during autotrophic growth (Fig. 6*E* and *SI Appendix*, Fig. S13*E*), indicating that overexpression of ribosomal proteins can enhance the autotrophic growth rate.

Finally, we confirmed whether the simultaneous suppression of the three target genes could synergistically increase autotrophic growth. For multiplexing transcriptional repression, the dCas12a-based CRISPRi system was employed because dCas12a can process its own crRNA and only requires the expression of a single CRISPR array, unlike dCas9 CRISPRi, which requires the independent expression of multiple sgRNAs (41). The dCas12a and guide RNA cassette targeting the three candidate genes were expressed in the multiplex strain, and we confirmed that their expression was simultaneously suppressed (<0.16-fold decrease, $P < 0.0001$, Student's *t* test) using quantitative RT–PCR (Fig. 6*F*). The simultaneous repression of several genes increased the specific growth rate four times than that of the control under autotrophic growth conditions ($P = 0.001$, Student's *t* test), and the maximum OD_{600} values also increased more than 1.7 times ($P = 0.0008$, Student's *t* test), showing a synergistic improvement in the acetogenesis phenotype (Fig. 6*G*). Furthermore, these results suggested that the multiplex strain exhibited higher volumetric productivity during acetogenesis than the wild-type strain. To demonstrate this, we constructed control acetoin (nontargeting array gRNA-dCas12a-acetoin biosynthesis pathway coexpression) and multiplex acetoin (multiplex gRNA targeting ELIM_c2976, ELIM_c1759, and ELIM_c1868–dCas12a–acetoin biosynthesis pathway coexpression) strains (Fig. 6*H*) using a previously validated acetoin biosynthetic pathway (40). Under CO_2-H_2 conditions, cell growth of the multiplex acetoin strain reached a plateau that was 1.8-fold higher than that of the control acetoin strain after 436 h. Similar to the volumetric productivity of acetate, acetoin was significantly increased (0.25 mM, 1.5-fold increase, $P = 0.009$, Student's *t* test) in the multiplex acetoin strain compared with the control acetoin strain (0.17 mM) after 436 h. Taken together, our CRISPRi screening approach demonstrated the ability to identify candidate genes that effectively enhanced autotrophic growth and biochemical production. It is difficult to effectively discover the targets for engineering autotrophic phenotype using genomic or other multiomics analyses.

Discussion

In this study, we conducted a CRISPRi screen to identify essential genes and potential mutations for improved autotrophic growth in the acetogenic bacterium, *E. limosum*, that were then validated by testing the phenotypes of the individual candidates. CRISPRi screening has an advantage over gene knockouts in that it can perturb key metabolic pathways and measure gene fitness (42). In the present study, acetogenesis-related genes in the W–L pathway, hydrogenase, the Rnf complex, and ATP synthase were found to be essential under CO_2-H_2 and syngas growth conditions at all passages (P1 to P3), except for formate dehydrogenase (ELIM_c2470–ELIM_c2472) (Fig. 3*A*). Although sgRNAs targeting formate dehydrogenase gradually depleted under autotrophic growth conditions (*SI Appendix*, Fig. S8*B*), they were not classified as essential genes (Fig. 3*A*). Instead, these results indicated that another formate dehydrogenase operon (ELIM_c1991–ELIM_c1993) was induced a twofold increase under autotrophic growth conditions when compared to the glucose condition (43), which compensated for the enzymatic reaction.

Although the required gene set for autotrophic growth has been identified in *C. autoethanogenum* (19), significant gaps remain in our understanding of the functions of other genes in heterotrophic and autotrophic acetogenesis. Under autotrophic growth conditions, the electrochemical sodium gradient across the cytoplasmic membrane is essential for cellular bioenergetics because the F_1F_0 ATP synthase and Rnf complex strictly rely only on the sodium ion potential (31, 44). Indeed, our CRISPRi screening revealed that the protein complex for membrane protein insertion/secretion and phosphatidic acid formation process for membrane lipid homeostasis were essential for autotrophic acetogenesis (Fig. 4*A*). Furthermore, our data suggest that long acyl-ACP concentration during phosphatidic acid biosynthesis was insufficient under autotrophic growth conditions. Based on their negative feedback regulation, we hypothesized that ACC, FabK, and FabH activities were inhibited when long-chain acyl-ACP is accumulated under heterotrophic growth conditions, further suggesting that the fitness of these genes was relatively high compared to that of other genes during phosphatidic acid biosynthesis (Fig. 4*C*). Conversely, genes encoding ACC, FabK, and FabH were essential for autotrophic growth, implying that they were not regulated by feedback inhibition. Optimal treatment of *E. coli* with cerulenin, an antibiotic that targets FabF, suppresses acyl-ACP elongation without inhibiting the initial condensing enzyme FabH, resulting in the decreased concentration of long-chain acyl-ACP (45, 46). In response to cerulenin treatment, the synthesis of short acyl-ACPs (4 to 10 carbon) by FabH was significantly increased, indicating that the fatty acid biosynthesis process by FabH is promoted when the concentration of long acyl-ACP is low.

Interestingly, our CRISPRi data also confirmed not only important membrane proteins such as the Rnf complex and F_1F_0 ATP synthase but also that those containing a high number of TMs were not required for autotrophic acetogenesis. We hypothesized that inhibition of ion channels/transporters benefited autotrophic growth by stabilizing the TM electrochemical ion gradient for efficient cellular bioenergetics and thus investigated the fitness of membrane proteins according to the number of TMs (Fig. 4*F*). According to a previous multiomics data analysis (9), TM proteins were translated with high efficiency under CO_2-H_2 conditions in *A. woodii;* however, when the expression of proteins containing a high number of TM domains (9 > TMs) was suppressed in our system, the growth rate significantly increased under both CO_2-H_2 and syngas growth conditions (Fig. 4*E*). These results suggested a design principle for constructing a bacterial strain for improving autotrophic growth by maintaining a stable TM electrochemical ion gradient through the elimination of membrane protein expression.

Most acetogenic bacteria exhibit high metabolic flexibility to utilize a variety of substrates and are therefore ubiquitously distributed in anoxic ecosystems. Unlike aerobic bacteria, which transfer electrons through NADH and unlimited oxygen, redox balancing is difficult and important in anaerobes because of the low redox potential of the electron acceptors. During substrate

oxidation, the W–L pathway contributes to CO_2 fixation and redox balance with energy conservation under heterotrophic growth conditions for more ATP gain (e.g., 4.3 ATP/mol glucose in *A. woodii*) than the conventional Embden–Meyerhof–Parnas pathway (2 mol ATP/mol glucose) (20). Based on transcriptional and translational data, we previously revealed that the W–L pathway contributes to CO_2 utilization and redox balancing with energy conservation via heterotrophic acetogenesis in *E. limosum* and *A. woodii* (9). CRISPRi screening also indicated that genes involved in the W–L pathway played an important role in heterotrophic growth under autotrophic conditions (Fig. 3*A*). However, TIS results in *C. autoethanogenum* showed that the W–L pathway was not essential in heterotrophic conditions (19), suggesting that the role of the W–L pathway among acetogenic strains may be different during heterotrophic growth.

CRISPRi data can also be used as a guide to enhance gas fermentation through strain engineering. Increasing gas–liquid mass transfer, optimizing medium and feed gas, and adding renewable electron sources have been attempted to improve productivity during gas fermentation, but meaningful enhancement of autotrophic growth rate has been achieved only through adaptive laboratory evolution (1.44-fold increase compared to the parental strain) under high CO concentration conditions (47). To identify gene candidates for enhancing autotrophic growth, we validated 12 knockdown strains and identified three repression clones ELIM_c2976 (1.98-fold increase), ELIM_c1795 (1.62-fold increase), and ELIM_c1868 (1.53-fold increase) that had significantly enhanced autotrophic growth rates ($P < 0.05$, Student's t test) when compared to the control strain (Fig. 6*B*). When they were repressed simultaneously by the dCas12a-based CRISPRi system, it was possible to induce a fourfold increase in the autotrophic growth rate compared to the control ($P < 0.001$, Student's t test). Thus, our CRISPRi screening method was useful for elucidating the principles for engineering gas-fermenting acetogenic bacteria.

Unexpectedly, the Rho factor encoded by ELIM_c1795 was a repression target for increasing the autotrophic growth rate. Rho-dependent transcriptional termination acts through the direct contact of RNA polymerase and Rho without a strong structure at the 3′-end. Unlike *E. coli*, where the *rho* gene is essential and about 50% of the transcription terminations are Rho dependent (48), the *rho* gene is not essential and does not seem to play an important role in *E. limosum* (*SI Appendix*, Fig. S12*A*) similar to observations reported in *B. subtilis* (49). Interestingly, the repression of *rho* affected the expression of methyl-branch, carbonyl-branch, and ATP synthase genes that have an I-shaped transcript 3′-end positions (TEP; U-lacking TEP, presumably Rho dependent) and an L-shaped TEP (U-rich TEP, Rho independent) (*SI Appendix*, Fig. S12 *B* and *C*). Although the inhibition of *rho* gene expression led to a decrease in its RNA levels under CO_2-H_2 conditions ($\log_2$ fold changes > −0.77 and $P_{adj} < 0.001$), it did not lead to a decrease in autotrophic growth (Fig. 6*B*). The results suggest that inhibition of *rho* expression enhanced autotrophic acetogenesis indirectly through induction of overexpression of fatty acid biosynthesis genes. Moreover, recent discovery of TEPs in *E. limosum* using Term-seq indicated a decrease in the dissociation of the Rho RNA polymerase under autotrophic conditions, suggesting that RNA polymerase and ribosomal proteins stall near the 3′-end during acetogenesis (40). Suppression of the *rho* gene contributed to overall autotrophic growth improvement by facilitating the reuse of effective RNA polymerase and ribosomal proteins by inhibiting the inefficient Rho-dependent RNA termination. Our results also suggested that ATP consumption was reduced by suppressing Rho-dependent transcription termination under autotrophic growth conditions, which increased the autotrophic growth rate.

In cluster I, 40.9% of genes were either transcription factors (TFs 18.2%; ELIM_c1740, ELIM_c1868, ELIM_c2379, and ELIM_c3084) or membrane proteins (22.7%; ELIM_c0077, ELIM_c0361, ELIM_c0539, ELIM_c0636, and ELIM_c1128); for example, the autotrophic growth rate was significantly increased (1.53-fold, $P < 0.01$, Mann–Whitney U test) during the repression of putative TF (ELIM_c1868). Furthermore, our data showed that membrane protein synthesis acted as a bottleneck for autotrophic growth. Therefore, our findings suggested that unknown genes regulated by putative TFs found in cluster I or membrane proteins could be candidates for knockdown/knockout to unlock autotrophic acetogenesis.

Collectively, the genome-wide CRISPRi approach was successfully used to screen for genotypes underlying heterotrophic/autotrophic growth–linked phenotypes. In this study, we unraveled gene fitness and identified unknown genes associated with improved autotrophic acetogenesis, the essentiality of heterotrophic acetogenesis, and mutants with an autotrophic growth advantage. These findings assist in understanding acetogenic metabolism and provide a platform for large-scale genome engineering of acetogenic bacteria.

Materials and Methods

Bacterial Strains, Growth Conditions, and DNA Manipulation. *E. limosum* American Type Culture Collection (ATCC) 8486 was obtained from the Leibniz Institute DSMZ-German Collection of Microorganisms and Cell Cultures (DSMZ, Braunschweig, Germany) and used in genome-scale CRISPRi experiments with the pJIR-sgRNA library. *E. limosum* and its derived mutant strains were cultivated strictly anaerobically at 37 °C with shaking at 180 rpm in DSMZ medium 135 supplemented with 2 g/L NaCl (Sigma-Aldrich, Burlington, MA) (22). Full details of the medium composition, culture conditions, and preparation of electrocompetent cells used in this work are described in *SI Appendix*, Materials and Methods.

Genome-Scale sgRNA Library. We have reported 170,691 sgRNAs with the least off-target effects on the *E. limosum* genome ATCC 8486 (CP019962) (22, 43). A total of 39,939 sgRNAs for 4,130 genes and 2,000 NT_sgRNA as negative controls were designed for genome-scale CRISPRi experiments. Full details of the genome-scale sgRNA library design and preparation of the sgRNA library are described in *SI Appendix*, Materials and Methods. All designed sgRNA sequences are listed in Dataset S1. The in-house Python scripts are available on our website (cholab.or.kr).

CRISPRi Screening Experiments. A schematic of the CRISPRi screening experiment is shown in *SI Appendix*, Fig. S1*B*. Full details of the transformation of CRISPRi library, CRISPRi screening, sequencing of NGS library of sgRNA, and NGS data processing and analysis of sgRNA libraries are described in *SI Appendix*, Materials and Methods.

Construction of Individual CRISPRi Mutants. The dCas9-based CRISPRi mutants were constructed in the same manner as CRISPRi libraries. To construct the pJIR-dCas9-*sgRNA*, sgRNA9405 (*folD*, ELIM_c0959), sgRNA16402 (*acsB*, ELIM_c1655), sgRNA16983 (*secD*, ELIM_c1731), sgRNA29199 (*accB*, ELIM_c2957), sgRNA29415 (ELIM_c2976), sgRNA17269 (ELIM_c1759), sgRNA18335 (ELIM_c1868), sgRNA22968 (ELIM_c2379), sgRNA37009 (ELIM_c3798), sgRNA176 (ELIM_c0044), sgRNA10735 (ELIM_c1100), sgRNA9371 (ELIM_c0955), sgRNA17083 (ELIM_c1740), sgRNA34040 (ELIM_c3476), sgRNA20041 (ELIM_c2041), and sgRNA18918 (ELIM_c1924) were used. NC1459 and NC1849 were used as the negative controls. Full details of the construction of multiplex CRISPRi mutants are described in *SI Appendix*, Materials and Methods. The oligonucleotide sequences of each *sgRNA#* are listed in Dataset S2. The oligonucleotide sequences used in this study are listed in Dataset S7.

qRT–PCR Assay. For total RNA extraction, 100 mL culture at an OD_{600} of 0.5 to 1.0 was harvested by centrifugation at 12,000 × *g* at 4 °C for 15 min. Total

RNA extraction and quantitative reverse-transcription polymerase chain reaction (qRT-PCR) were performed as described (22). The primers used for qRT–PCR are listed in Dataset S7. The *gyrA* gene (ELIM_c0629), which encodes the DNA gyrase subunit A, was used as an endogenous control.

Transcriptome Analysis. Biological duplicates of cell cultures were collected at a midexponential phase (OD_{600} of 0.2 to 0.4) by centrifugation at 12,000 × *g* at 4 °C for 15 min. Total RNA was extracted from the collected cells as previously described (22). Ribosomal RNA and genomic DNA contaminants were removed using the RiboRid method (50). Briefly, custom-designed oligonucleotide primers complementary to *E. limosum* ribosomal RNA (anti-rRNA oligonucleotide probes) were hybridized with target rRNA transcripts in the total RNA sample before 10 U RNase H was added to specifically degrade the RNA strand of RNA:DNA heteroduplexes, and 12 U DNase I was added to remove gDNA fragments and primer dimers. The anti-rRNA oligonucleotide probes were reported in a previous study (50). Full details of the construction of RNA-seq library and transcriptome analysis are described in *SI Appendix*, Materials and Methods.

Metabolite Measurement. The metabolites were measured using high-performance liquid chromatography (Shimadzu, Kyoto, Japan) equipped with a refractive index detector and a MetaCarb 87 H 300 × 7.8 mm column (Agilent Technologies). Full details of the metabolite measurement are described in *SI Appendix*, Materials and Methods.

Statistical Analyses. Data were analyzed, and statistical testing (Pearson's correlation coefficient, two-tailed Student's *t* test, Wilcoxon signed-rank test, and Wilcoxon–Mann–Whitney test) performed in Anaconda (https://www.anaconda.com/) and GraphPad Prism v8 software (GraphPad, San Diego, CA). *P* values < 0.05 were considered statistically significant.

Data, Materials, and Software Availability. Raw sequencing reads from CRISPRi screens are available at the European Nucleotide Archive (ENA) under accession number PRJEB49804 (51). Raw read counts, Z_{sgRNA} values, and gene fitness values for each CRISPRi screen are shown in Datasets S1, S3, and S4, respectively. The normalized RNA levels for CRISPRi mutants are provided in Dataset S5. Raw Illumina RNA-seq reads are available at the SRA under accession number PRJNA850027 (52).

ACKNOWLEDGMENTS. This work was supported by the C1 Gas Refinery Program (2018M3D3A1A01055733 to B.-K.C.) through the National Research Foundation of Korea (NRF) funded by the Ministry of Science and ICT.

Author affiliations: [a]Department of Biological Sciences, Korea Advanced Institute of Science and Technology, Daejeon 34141, Republic of Korea; and [b]KAIST Institutes for the BioCentury, Korea Advanced Institute of Science and Technology, Daejeon 34141, Republic of Korea

1. K. Schuchmann, V. Müller, Autotrophy at the thermodynamic limit of life: A model for energy conservation in acetogenic bacteria. *Nat. Rev. Microbiol.* **12**, 809–821 (2014).
2. A. G. Fast, E. T. Papoutsakis, Stoichiometric and energetic analyses of non-photosynthetic CO2-fixation pathways to support synthetic biology strategies for production of fuels and chemicals. *Curr. Opin. Chem. Eng.* **1**, 380–395 (2012).
3. M. J. McInerney, M. P. Bryant, *Biomass Conversion Processes for Energy and Fuels* (Springer, New York, NY, 1981), pp. 277–296.
4. F. E. Liew *et al.*, Carbon-negative production of acetone and isopropanol by gas fermentation at industrial pilot scale. *Nat. Biotechnol.* **40**, 335–344 (2022).
5. M. Köpke, S. D. Simpson, Pollution to products: Recycling of 'above ground' carbon by gas fermentation. *Curr. Opin. Biotech.* **65**, 180–189 (2020).
6. H. Roh *et al.*, Complete genome sequence of a carbon monoxide-utilizing acetogen, eubacterium limosum KIST612. *J. Bacteriol.* **193**, 307–308 (2011).
7. W. J. Kelly *et al.*, The complete genome sequence of Eubacterium limosum SA11, a metabolically versatile rumen acetogen. *Stand. Genomic. Sci.* **11**, 26 (2016).
8. Y. Song *et al.*, Determination of the genome and primary transcriptome of syngas fermenting eubacterium limosum ATCC 8486. *Sci. Rep.* **7**, 13694 (2017).
9. J. Shin *et al.*, Genome-scale analysis of Acetobacterium woodii identifies translational regulation of acetogenesis. *mSystems* **6**, e00696-21 (2021).
10. K. Valgepea *et al.*, Absolute proteome quantification in the gas-fermenting acetogen Clostridium autoethanogenum. *mSystems* **7**, e00026-22 (2022).
11. S. Jin *et al.*, Synthetic biology on acetogenic bacteria for highly efficient conversion of C1 gases to biochemicals. *Int. J. Mol. Sci.* **21**, 7639 (2020).
12. W. Jiang, D. Bikard, D. Cox, F. Zhang, L. A. Marraffini, RNA-guided editing of bacterial genomes using CRISPR-Cas systems. *Nat. Biotechnol.* **31**, 233 (2013).
13. W. Jiang, P. Oikonomou, S. Tavazoie, Comprehensive genome-wide perturbations via CRISPR adaptation reveal complex genetics of antibiotic sensitivity. *Cell* **180**, 1002–1017.e31 (2020).
14. L. Yao *et al.*, Pooled CRISPRi screening of the cyanobacterium Synechocystis sp PCC 6803 for enhanced industrial phenotypes. *Nat. Commun.* **11**, 1666 (2020).
15. H. H. Lee *et al.*, Functional genomics of the rapidly replicating bacterium Vibrio natriegens by CRISPRi. *Nat. Microbiol.* **4**, 1105–1113 (2019).
16. F. Rousset *et al.*, Genome-wide CRISPR-dCas9 screens in E. coli identify essential genes and phage host factors. *Plos Genet.* **14**, e1007749 (2018).
17. F. Rousset *et al.*, The impact of genetic diversity on gene essentiality within the Escherichia coli species. *Nat. Microbiol.* **6**, 301–312 (2021).
18. T. Wang *et al.*, Pooled CRISPR interference screening enables genome-scale functional genomics study in bacteria with superior performance. *Nat. Commun.* **9**, 2475 (2018).
19. C. Woods *et al.*, Required gene set for autotrophic growth of Clostridium autoethanogenum. *Appl. Environ. Microb.* **88**, e02479-21 (2022).
20. K. Schuchmann, V. Müller, Energetics and application of heterotrophy in acetogenic bacteria. *Appl. Environ. Microb.* **82**, 4056–4069 (2016).
21. A. Katsyv, V. Müller, Overcoming energetic barriers in acetogenic C1 conversion. *Front. Bioeng. Biotechnol.* **8**, 621166 (2020).
22. J. Shin *et al.*, Genome engineering of eubacterium limosum using expanded genetic tools and the CRISPR-Cas9 system. *Acs. Synth. Biol.* **8**, 2059–2068 (2019).
23. R. H. Michna, B. Zhu, U. Mäder, J. Stülke, SubtiWiki 2.0–An integrated database for the model organism Bacillus subtilis. *Nucleic Acids Res.* **44**, D654–D662 (2016).
24. H. S. Girgis, Y. Liu, W. S. Ryu, S. Tavazoie, A comprehensive genetic characterization of bacterial motility. *Plos Genet.* **3**, e154 (2007).
25. U. Mäder, A. G. Schmeisky, L. A. Flórez, J. Stülke, SubtiWiki–A comprehensive community resource for the model organism Bacillus subtilis. *Nucleic Acids Res.* **40**, D1278–D1287 (2012).
26. M. Dembek *et al.*, High-throughput analysis of gene essentiality and sporulation in Clostridium difficile. *mBio* **6**, e02383-14 (2015).
27. Y. Yamazaki, H. Niki, J. Kato, Microbial gene essentiality: Protocols and bioinformatics. *Methods Mol. Biol.* **416**, 385–389 (2008).
28. Y.-M. Zhang, C. O. Rock, Membrane lipid homeostasis in bacteria. *Nat. Rev. Microbiol.* **6**, 222–233 (2008).
29. T. Tsukazaki *et al.*, Structure and function of a membrane component SecDF that enhances protein export. *Nature* **474**, 235–238 (2011).
30. R. J. Schulze *et al.*, Membrane protein insertion and proton-motive-force-dependent secretion through the bacterial holo-translocon SecYEG–SecDF–YajC–YidC. *Proc. Natl. Acad. Sci. U.S.A.* **111**, 4844–4849 (2014).
31. J. Jeong *et al.*, Energy conservation model based on genomic and experimental analyses of a carbon monoxide-utilizing, butyrate-forming acetogen, Eubacterium limosum KIST612. *Appl. Environ. Microbiol.* **81**, 4782–4790 (2015).
32. I. S. Chang, B. H. Kim, R. W. Lovitt, J. S. Bang, Effect of CO partial pressure on cell-recycled continuous CO fermentation by Eubacterium limosum KIST612. *Process Biochem.* **37**, 411–421 (2001).
33. S. Park *et al.*, Acetate-assisted increase of butyrate production by Eubacterium limosum KIST612 during carbon monoxide fermentation. *Bioresource Technol.* **245**, 560–566 (2017).
34. M. J. Kerner *et al.*, Proteome-wide analysis of chaperonin-dependent protein folding in Escherichia coli. *Cell* **122**, 209–220 (2005).
35. E. S. Bochkareva, M. E. Solovieva, A. S. Girshovich, Targeting of GroEL to SecA on the cytoplasmic membrane of Escherichia coli. *Proc. Natl. Acad. Sci. U.S.A.* **95**, 478–483 (1998).
36. A. Hoffmann, B. Bukau, G. Kramer, Structure and function of the molecular chaperone Trigger factor. *Biochim. Biophys. Acta* **1803**, 650–661 (2010).
37. W. Baumeister, J. Walz, F. Zühl, E. Seemüller, The proteasome: Paradigm of a self-compartmentalizing protease. *Cell* **92**, 367–380 (1998).
38. S. Simpson, M. Koepke, F. Liew, "Recombinant microorganisms and methods of use thereof." US20110256600A1 (2011).
39. G. Yang *et al.*, Rapid generation of universal synthetic promoters for controlled gene expression in both gas-fermenting and Saccharolytic Clostridium species. *Acs. Synth. Biol.* **6**, 1672–1678 (2017).
40. Y. Song *et al.*, Development of highly characterized genetic bioparts for efficient gene expression in CO2-fixing Eubacterium limosum. *Metab. Eng.* **72**, 215–226 (2022).
41. X. Zhang *et al.*, Multiplex gene regulation by CRISPR-ddCpf1. *Cell Discov.* **3**, 17018 (2017).
42. D. Beuter *et al.*, Selective enrichment of slow-growing bacteria in a metabolism-wide CRISPRi library with a TIMER protein. *Acs. Synth. Biol.* **7**, 2775–2782 (2018).
43. Y. Song *et al.*, Genome-scale analysis of syngas fermenting acetogenic bacteria reveals the translational regulation for its autotrophic growth. *BMC Genom.* **19**, 837 (2018).
44. D. Litty, V. Müller, A Na+ A1AO ATP synthase with a V-type c subunit in a mesophilic bacterium. *FEBS J.* **287**, 3012–3023 (2020).
45. S. Jackowski, C. O. Rock, Acetoacetyl-acyl carrier protein synthase, a potential regulator of fatty acid biosynthesis in bacteria. *J. Biol. Chem.* **262**, 7927–7931 (1987).
46. J. P. Torella *et al.*, Tailored fatty acid synthesis via dynamic control of fatty acid elongation. *Proc. Natl. Acad. Sci. U.S.A.* **110**, 11290–11295 (2013).
47. S. Kang *et al.*, Adaptive laboratory evolution of Eubacterium limosum ATCC 8486 on carbon monoxide. *Front. Microbiol.* **11**, 402 (2020).
48. C. J. Cardinale *et al.*, Termination factor rho and its cofactors NusA and NusG silence foreign DNA in E. coli. *Science* **320**, 935–938 (2008).
49. C. J. Ingham, J. Dennis, P. A. Furneaux, Autogenous regulation of transcription termination factor Rho and the requirement for Nus factors in Bacillus subtilis. *Mol. Microbiol.* **31**, 651–663 (1999).
50. D. Choe *et al.*, RiboRid: A low cost, advanced, and ultra-efficient method to remove ribosomal RNA for bacterial transcriptomics. *Plos Genet.* **17**, e1009821 (2021).
51. J. Shin *et al.*, Genome-wide CRISPRi screening of Eubacterium limosum. The European Nucleotide Archive. https://www.ebi.ac.uk/ena/browser/view/PRJEB49804. Deposited 31 May 2022.
52. J. Shin *et al.*, RNA-seq of E. limosum CRISPRi mutants. NCBI Sequence Read Archive. https://www.ncbi.nlm.nih.gov/sra/?term=PRJNA850027. Deposited 16 June 2022.